Raman Spectroscopy of Lithium Niobite ($LiNbO_2$)

S. A. Howard,[a,*] E. Evlyukhin,[a] S. Abdel Razek,[a] G. J. Paez Fajardo,[a] M. J. Wahila,[a] T. M. McCrone,[b] W. A. Doolittle,[b] W-C. Lee,[a] L. F. J. Piper[c]

[a]*Department of Physics, Applied Physics and Astronomy, Binghamton University, Binghamton, New York 13902, USA*
[b]*School of Electrical and Computer Engineering, Georgia Institute of Technology, Atlanta, Georgia 30332, USA*
[c]*WMG, University of Warwick, Coventry, CV4 7AL, United Kingdom*

Abstract

Lithium niobite ($LiNbO_2$) single crystals fabricated via liquid phase electro-epitaxy are studied by Raman spectroscopy. We present the Raman spectra of the pristine and chemically delithiated $LiNbO_2$ crystals under ambient conditions. Two characteristic experimental Raman peaks located at 456 cm^{-1} and 640 cm^{-1} are assigned to the O E_{2g} and O A_{1g} phonon modes respectively, as determined from first principles-based calculations. Furthermore, by chemically delithiating the crystals it is shown that the spectral changes of the O E_{2g} can be used to capture lithium content variation within the structure.

Functional oxide memristors have the potential to revolutionize neuromorphic computing, which aims to mimic the operation of biological brains using artificial circuits.[1] While neuromorphic systems can be implemented with traditional CMOS circuitry, this requires many conventional nanoscale transistors, resulting in significant power consumption and scalability issues.[9-11] The development of neuromorphic computing rests on understanding the underlying physics of memristors, which are the crucial building blocks of tangible neuromorphic devices. The typical memristor reported is a two terminal device that switches digitally from a high resistance state to a low resistance through a complex combination of processes (e.g., redox reactions (amorphous materials),[2,3] ionic transport (cathode materials),[4] metal-to-insulator-transition materials,[5,6] etc.)
Lithium niobite ($LiNbO_2$), previously studied due to properties such as superconductivity,[7] has recently shown great potential for memristive applications.[8,9] Traditional filamentary devices typically require the migration of O^{2-} ions to form narrow conductive channels and access discrete resistive states whereas, the resistive states of $LiNbO_2$ are analog in nature and are thought to be modulated by a more uniform diffusion of Li^+ ions through its layered crystal structure.[10] This more uniform ion diffusion mechanism may help overcome some of the major disadvantages of traditional memristors, such as the need for an initial preforming/electroforming process to breakdown or otherwise alter the as-deposited material before the device can function.[11] $LiNbO_2$ has been shown to switch with very low power/voltage with nanovolt switching predicted when scaled. Additionally, unlike other memristor technologies, the memristance value can be engineered similarly to CMOS design rules based on device geometry and both volatile and non-volatile operation can be achieved in the same material simply by changing the fabrication process.[9] In terms of developing a biomimetic functionality the nonvolatile and analog behavior of $LiNbO_2$ memristors can potentially enable learning in neuromorphic circuits.
Previously, we have investigated the intrinsic properties responsible for the analog memristive behavior of $LiNbO_2$ single crystals.[4] Using x-ray absorption spectroscopy together with the first-principles x-ray spectroscopic simulations, we have determined that depopulation of the Nb $4d_z^2$ orbital upon chemical delithiation (Li^+ ion extraction) could be considered as the main mechanism

of the analog response. The intercalation mechanism of $LiNbO_2$-based devices which is described via a lithium content profile requires comprehensive analysis of the lithium concentration variations across the device. We should note that lithium ions are not straightforward to characterize with x-ray experiments in contrast to transition metals, due to lithium's drastically low electron concentration in its electronic clouds. Thus, experiments in the visible range which are also sensitive to structural variations such as Raman spectroscopy are necessary. Indeed, Raman spectroscopy is a powerful tool for the investigation of structural and local environment transformations in organic/inorganic materials.[12,13] Although there have been theoretical predictions of the vibrational properties of $LiNbO_2$,[14] no Raman measurements have been reported in the literature for this compound.

We note that Raman mapping could provide the lithium content profile across the device in in-situ and operando measurements.

This work reports on the Raman study of high quality $LiNbO_2$ single crystals and compares it to theoretical simulations. High-quality single crystals were grown using liquid phase electro-epitaxy (LPEE). The detailed discussion of the fabrication process is found elswhere.[15] Moreover, through chemical delithiation we demonstrate the spectroscopic variation that can be used to monitor Li ion intercalation occurring in active layer $LiNbO_2$ based memristors.

Fig. 1 shows the image of a $LiNbO_2$ single crystal. The crystal is burgundy red in color which is consistent with previously reported references and was explained by band gap of ~2.0 eV.[16,17] $LiNbO_2$ is similar structurally to several lithium ion battery cathode materials such as lithium cobalt oxide ($LiCoO_2$).[18] In general, these materials have a layered structure in which planes of lithium ions are separated by sheets of metal oxide as shown on the right of Fig. 1. The primary structural difference between lithium niobite and other battery cathode materials is a 180° twist in the crystal structure. This results in the niobium atoms occupying trigonal-prismatic sites in $LiNbO_2$ (space group $P6_3/mmc$) and consequently a higher degree of metal-metal orbital overlap.[19] Generally, it is thought that the tunable electrical and optical properties that make $LiNbO_2$ useful for neuromorphic computing result from lithium variations within the structure.[9,20]

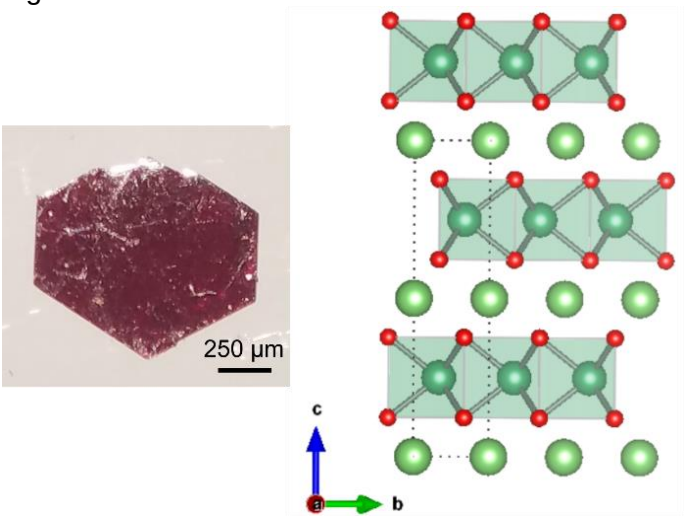

FIG. 1. On the left is an image of $LiNbO_2$ single crystal displaying burgundy color. The right image is a schematic of the hexagonal $P6_3/mmc$ crystal structure (red, dark green and light green spheres correspond to oxygen niobium and lithium atoms, respectively).

Raman spectra were obtained using a Renishaw inVia micro-Raman spectrometer equipped with a high power near-infrared diode laser (λ = 785 nm) to excite the sample and spectra recorded in

backscattering geometry. The spectra were obtained at a laser power set to approximately 15 mW, collected over a range of 100-1000 cm^{-1} at room temperature. Fig. 2 shows the experimental Raman spectrum of a $LiNbO_2$ single crystal.

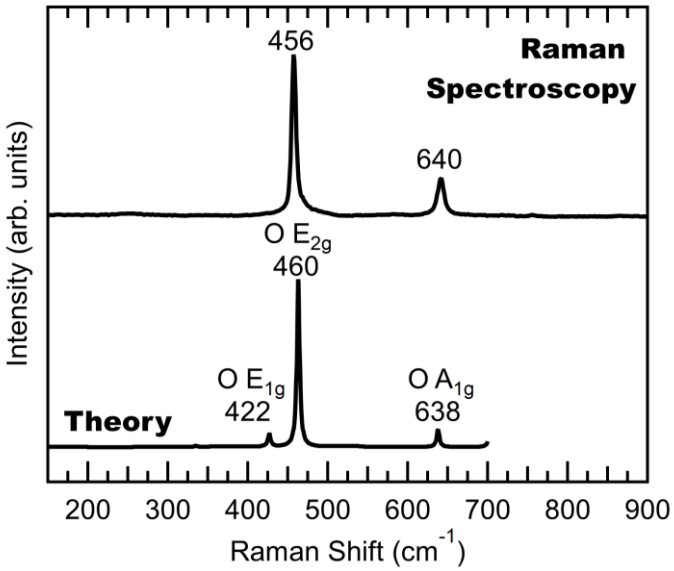

FIG. 2. Experimentally and theoretically obtained Raman spectra of pristine $LiNbO_2$. Simulated spectrum exhibits four Raman active peaks (three shown) attributed to the Nb E_{2g}, O E_{1g}, O E_{2g} and O A_{1g}.

As shown in the top spectrum of Fig. 2, There are two characteristic peaks observed in the experimental Raman spectroscopy at 456 cm^{-1} and 640 cm^{-1}. It should be noted that we also detected significantly less intense peaks that can be attributed to slight impurities within the crystal and are presented in the supplementary material (Fig. S1). For understanding the nature of the two characteristic spectral features we employed first principles-based calculations. Crystal structure information of stoichiometric $LiNbO_2$ was retrieved from a previous study by Bordet et. al..[17] A 2x2x2 supercell which contained 8 Li, 8 Nb, and 16 O was constructed to obtain a relaxed structure. A typical ion-electron relaxation process was performed using the Vienna *Ab- Initio* simulation package (VASP) code[21] under the projector augmented-wave (PAW)[22,23] and the local density approximation (LDA).[24] Then the relaxed structure was used to construct an even larger 2x2x2 supercell that contained 32 Li, 32 Nb and 64 O atoms for phonon calculations. The phonon calculations were performed using small displacements of the atoms in the supercell as implemented in the Phonopy pre-processing module. Total phonon density of states (see supplementary information Fig. S3) data was generated from the VASP output using a 3x3x5 Γ centered Monkhorst-Pack grids. The number of bands raised to 576, the cutoff energy remained fixed at 650 eV, and the global break condition for the electronic SC-loop was set at 10^{-8} as recommended by Phonopy.[25] Raman simulations also were performed using the local density approximation (LDA) as implemented in the Quantum-Espresso (QE) code.[26] Norm conserving pseudopotentials were used with a plane wave cutoff energy of 100 Ry to describe the interaction between ions and electrons. The calculation was done for a supercell 2 x 2 x 2 using a 8 x 8 x 8 Γ centered grids. The simulated Raman spectrum captures four Raman active Nb- and O-vibrational modes for stoichiometric $LiNbO_2$. These spectral features are related to Nb E_{2g} at 53.5 cm^{-1}, O E_{1g} at 422 cm^{-1}, O E_{2g} at 458 cm^{-1} and O A_{1g} at 638 cm^{-1}. A list of the vibrational modes can be found in Fig. S2. We note that Nb E_{2g} and the O E_{1g} peak were not captured in the experimental spectra due to low resolution. Moreover, as can be seen in Fig. 2 the simulated

Raman spectrum reveals that the O E_{1g} is approximately 2 orders of magnitude in intensity smaller than the O E_{2g}. VASP with Phonopy-Spectroscopy package is used for calculating the Raman spectra and compared with spectra using QE as shown in Fig.S3. Both spectra have the same peak but the peak intensity of O E_{1g} in QE is larger than VASP. In VASP, Raman active mode were computed as follows: the static dielectric matrix of the selected modes was computed in VASP using density functional perturbation theory with a 5x5x5 Γ centered Monkhorst-Pack grid, energy cutoff was at 650 eV, with 144 bands, an electronic self-consistent break at 10^{-8}, and the number of bands that are treated in parallel was set at the VASP default value. We note that the Raman simulations were performed prior to experimental measurements. Therefore, the experimental Raman peaks can be assigned as the O E_{2g} and O A_{1g} phonon modes.

The Raman spectroscopic changes associated with chemical delithiation of $LiNbO_2$ single crystals were further examined. A single crystal was soaked in a 37% HCl aqueous bath at room temperature for 19 h and dried with nitrogen following the bath.[4] HCL soaking was previously determined to remove Li+ ions from $LiNbO_2$ via various chemically specific x-ray spectroscopic[4] and x-ray diffraction[28] studies. The Raman spectrum of the soaked crystal was collected at the same measurement parameters discussed above and depicted in Fig. 3.

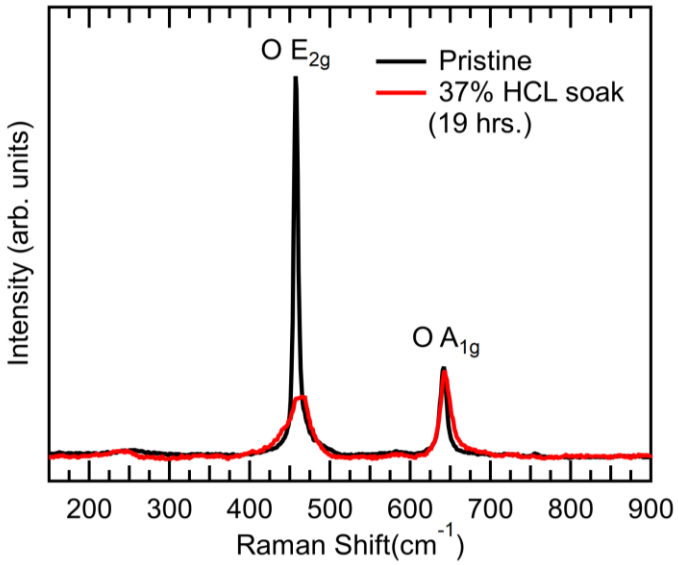

FIG. 3. Raman spectra of pristine and HCl soaked $LiNbO_2$ single crystal normalized to the O A_{1g} peak

After the HCl soaking a large decrease in the O E_{2g} peak intensity relative to the O A_{1g} is observed. The decrease in the O E2g is associated with the delithiation of the crystal. It was previously observed with extended x-ray absorption fine structure measurements that HCl-induced delithiation causes the interlayer distance between oxygen and niobium ions within the trigonal prismatic coordination to shrink from 2.157 Å to 2.115 Å. Hence, any change in the Nb-O bond length has an impact on the O electronic structure. This impact induces changes to polarizability, which ultimately impacts the phonon modes and Raman sensitivity of symmetries along the c-axis (O E_{2g}). We note that the Raman measurements were highly spot sensitive for the HCL soaked sample. This can be explained by the layered structure of $LiNbO_2$ (Fig. 1), which shows that the Li ions are specifically oriented along *a-b* plane where intercalation/deintercalation between the sheets of Nb-O trigonal prismatic sites takes place. It was determined in our previous work that the crystals are highly (0001) oriented with step edges that have flat regions which are

roughly ~1-10 micrometers wide that exhibit RMS roughnesses of 1.67nm.[15] Given this, we suggest that the chemical delithiation from the HCL will occur near the edge of the macroscopic steps. Thus, the interaction between the HCL and the crystal surface is expected to be different at various locations of the crystal. For this reason, we measured Raman spectra on multiple spots on the same crystal before and after HCl soaking (see supporting information Fig. S5). It was found that all spots on the pristine sample exhibit the same spectrum as shown in Fig 2. Whereas for the HCl soaked sample some spots displayed pristine spectra while others showed the dramatic decrease in the O E_{2g} peak even after 1 week. Notably, however, the inhomogeneous delithiation throughout the crystal is consistent with the fact that the crystal did not change color. In fact, it was observed that by chemically delithiating thin film Li_xNbO_2 from x = 0.93 to x = 0.45 the color of the film changed from a transparent burgundy-red color to transparent green-olive.[27] The maximum observed delithiation via HCL soaking was 31% as observed by Moshopoulou et al.[28] Hence, as a qualitative estimate, the delithiation observed after 1 day of HCL soaking is marginal throughout the crystal i.e. the majority of the film remained nearly stoichiometric. Moreover, the presence of a Raman signal at all indicates that the delithiated crystal does not undergo a complete metal to insulator transition. This is opposed to a similar intercalation based material, $LiCoO_2$, which showed an overall decrease to a complete loss in the Raman intensity of its characteristic Eg and A1g bands due to 3 order of magnitude increase in conductivity at 20% delithiation.[29,30] This is in agreement with our previous x-ray spectroscopic studies that showed that removing Li^+ via HCL chemical soaking oxidizes the Nb and depopulates the top Nb d-states within the valence band thus, facilitating the onset of p-type conduction prior to metallicity.[4] Hence, the decrease in the O E_{2g} peak intensity is due to reduced Li content in the HCl soaked $LiNbO_2$ crystal. The analog switching behavior of $LiNbO_2$ which is based on the diffusion of Li^+ ions would enable the ability to control the resistive states of a memristive device which is critical for neuromorphic applications. Therefore, the aforementioned spectral change could be used to perform operando and in-situ Raman mapping on $LiNbO_2$-based devices to quantify correlation of Li-concentration with $LiNbO_2$ analog memristance.

In conclusion, we have presented Raman spectra of $LiNbO_2$ single crystals. Comparison with theoretical Raman simulations allowed us to assign two characteristic phonon modes as the O E_{2g} and O A_{1g} peaks which are located at 456 and 640 cm^{-1}, respectively. Moreover, through chemical delithiation of the crystal a large decrease in the O E_{2g} peak intensity relative to the O A_{1g} was observed. This spectral change can be used to benchmark Li variation across well-defined $LiNbO_2$ based memristive devices for future neuromorphic applications.

This material is based on work supported by the Air Force Office of Scientific Research under Grant FA9550-18-1-0024 administered by Dr. Ali Sayir.

[1] C. Sung, H. Hwang, and I.K. Yoo, J. Appl. Phys. **124**, 151903 (2018).

[2] C. Li, B. Gao, Y. Yao, X. Guan, X. Shen, Y. Wang, P. Huang, L. Liu, X. Liu, J. Li, C. Gu, J. Kang, and R. Yu, Adv. Mater. **29**, 1602976 (2017).

[3] J.C. Shank, M. Brooks Tellekamp, M.J. Wahila, S. Howard, A.S. Weidenbach, B. Zivasatienraj, L.F.J. Piper, and & W.A. Doolittle, Sci. Rep. **8**, 12935 (2018).

[4] S.A. Howard, C.N. Singh, G.J. Paez, M.J. Wahila, L.W. Wangoh, S. Sallis, K. Tirpak, Y. Liang, D. Prendergast, M. Zuba, J. Rana, A. Weidenbach, T.M. McCrone, W. Yang, T.L. Lee, F. Rodolakis, W. Doolittle, W.C. Lee, and L.F.J. Piper, APL Mater. **7**, 071103 (2019).

[5] S.A. Howard, E. Evlyukhin, G. Páez Fajardo, H. Paik, D.G. Schlom, and L.F.J. Piper, Adv. Mater. Interfaces **8**, 2001790 (2021).

[6] G.J. Páez Fajardo, S.A. Howard, E. Evlyukhin, M.J. Wahila, W.R. Mondal, M. Zuba, J.E. Boschker, H. Paik, D.G. Schlom, J.T. Sadowski, S.A. Tenney, B. Reinhart, W.C. Lee, and L.F.J. Piper, Chem. Mater. **33**, 1416 (2021).

[7] M.J. Geselbracht, A.M. Stacy, and M. Rosseinsky, *Lithium Niobium Oxide: LiNbO2 and Superconducting LiXNbO2* (Inorganic Synthesis, 1995).

[8] J.D. Greenlee, W.L. Calley, W. Henderson, and W.A. Doolittle, Phys. Status Solidi **9**, 155 (2012).

[9] B. Zivasatienraj, M. Brooks Tellekamp, A.S. Weidenbach, A. Ghosh, T.M. McCrone, and W. Alan Doolittle, J. Appl. Phys. **127**, (2020).

[10] J.D. Greenlee, C.F. Petersburg, W. Laws Calley, C. Jaye, D.A. Fischer, F.M. Alamgir, and W. Alan Doolittle, Appl. Phys. Lett. **100**, 182106 (2012).

[11] J. Joshua Yang, F. Miao, M.D. Pickett, D.A.A. Ohlberg, D.R. Stewart, C.N. Lau, and R.S. Williams, Nanotechnology **20**, 215201 (2009).

[12] E. Evlyukhin, S.A. Howard, H. Paik, G.J. Paez, D.J. Gosztola, C.N. Singh, D.G. Schlom, W.-C. Lee, and L.F.J. Piper, Nanoscale **12**, 18857 (2020).

[13] E. Evlyukhin, L. Museur, M. Traore, S.M. Nikitin, A. Zerr, and A. Kanaev, J. Phys. Chem. B **119**, 3577 (2015).

[14] E.R. Ylvisaker and W.E. Pickett, Phys. Rev. B **74**, 075104 (2006).

[15] J.D. Greenlee, J.C. Shank, M.B. Tellekamp, B.P. Gunning, C.A.M. Fabien, and W.A. Doolittle, Cryst. Growth Des. **14**, 2218 (2014).

[16] M.J. Geselbracht, A.M. Stacy, A.R. Garcia, B.G. Silbernagel, and G.H. Kwei, J. Phys. Chem. **97**, 7102 (1993).

[17] P. Bordet, E. Moshopoulou, S. Liesert, J.J. Capponi, and T.E. Microscopy, **240**, 745 (1994).

[18] J. Van Elp, J.L. Wieland, H. Eskes, P. Kuiper, G.A. Sawatzky, F.M.F. De Groot, and T.S. Turner, Phys. Rev. B **44**, 6090 (1991).

[19] G. Meyer and R. Hoppe, J. Less-Common Met. **46**, 55 (1976).

[20] S.A. Howard, C.N. Singh, G.J. Paez, M.J. Wahila, L.W. Wangoh, S. Sallis, K. Tirpak, Y. Liang, D. Prendergast, M. Zuba, J. Rana, A. Weidenbach, T.M. McCrone, W. Yang, T.-L. Lee, F. Rodolakis, W. Doolittle, W.-C. Lee, and L.F.J. Piper, APL Mater. **7**, 071103 (2019).

[21] G. Kresse and J. Furthmüller, Phys. Rev. B - Condens. Matter Mater. Phys. **54**, 11169 (1996).

[22] P.E. Blöchl, Phys. Rev. B **50**, 17953 (1994).

[23] D. Joubert, Phys. Rev. B - Condens. Matter Mater. Phys. **59**, 1758 (1999).

[24] J.P. Perdew, K. Burke, and M. Ernzerhof, Phys. Rev. Lett. **77**, 3865 (1996).

[25] A. Togo and I. Tanaka, Scr. Mater. **108**, 1 (2015).

[26] G. Paolo, B. Stefano, B. Nicola, C. Matteo, C. Roberto, C. Carlo, C. Davide, L.C. Guido, C.

Matteo, D. Ismaila, C. Andrea Dal, G. Stefano de, F. Stefano, F. Guido, G. Ralph, G. Uwe, G. Christos, K. Anton, L. Michele, M.-S. Layla, M. Nicola, M. Francesco, M. Riccardo, P. Stefano, P. Alfredo, P. Lorenzo, S. Carlo, S. Sandro, S. Gabriele, P.S. Ari, S. Alexander, U. Paolo, and M.W. Renata, J. Phys. Condens. Matter **21**, 399502 (2009).

[27] T. Soma, K. Yoshimatsu, and A. Ohtomo, Science Advance **6**, (2020).

[28] E. G. Moshopoulou, P. Bordet, and J. J. Capponi, Phys. Rev. B - Condens. Matter Mater. Phys. **59**, 9590 (1999).

[29] M. Inaba, Y. Iriyama, Z. Ogumi, Y. Todzuka, and A. Tasaka, J. Raman Spectroscopy **28**, 613 (1997).

[30] E. Flores, N. Mozhzhukhina, U. Aschauer, and E. J. Berg, ACS Appl. Mater. Interfaces **13**, 22540 (2021).